Fully nonlinear global modes in slowly varying flows

A. Couairon and J.-M. Chomaz
Laboratoire d'Hydrodynamique (LadHyX), CNRS UMR 7646, École Polytechnique,
F-91128 Palaiseau, France

We study the existence of nonlinear solutions of the real Ginzburg–Landau amplitude equation, with varying coefficients when the solution is subject to a boundary condition at $x=0$. These solutions, called nonlinear global modes, are explicitly obtained from a matched asymptotic expansion when nonlinear effect dominates over the inhomogeneity. The dynamics of this model is believed to mimic the behavior of strongly nonlinear but weakly nonparallel basic flow (basic flow varying in the streamwise direction). For the model, we derive scaling laws for the amplitude of nonlinear global modes and for the position of the maximum that explain for the first time the experimental observations of Goujon-Durand *et al.* [Phys. Rev. E **50**, 308 (1994)] and the numerical simulations of Zielinska and Wesfreid [Phys. Fluids **7**, 1418 (1995)] of the wake behind bluff bodies. © *1999 American Institute of Physics.* [S1070-6631(99)03111-6]

I. INTRODUCTION

Spatially extended open flows may be classified according to their dynamical behavior. Either they may be easily manipulated by external excitations (for example, a forcing fixed in space or upstream noise contaminating the entrance condition of the flow) and they behave as a noise amplifier. Jets, mixing layers, and boundary layers belong to this class. Or they display a self-sustained saturated oscillation nearly unaltered by external excitation. In this case, the flow becomes tuned at a specific intrinsic frequency everywhere in space and behaves as an oscillator. The associated spatial distribution of fluctuations defines the global mode of the flow.[1] The Kármán vortex street behind a cylinder constitutes a typical example of transition to a global mode regime. When the Reynolds number is increased above a critical value (~ 47), the laminar steady flow becomes globally unstable and ultimately exhibits a self sustained oscillation (a saturated limit cycle oscillation[2–5]). A global mode regime (also called a self-sustained oscillation regime or a resonant regime) appears in jets,[6] when the inner density is lightened; in mixing layer when suction is applied to one of the stream;[7] in Rayleigh–Bénard with Poiseuille flow when the heating is high enough;[8,9] or in Taylor-Couette system with an added axial throughflow,[10] when the rotation rate is increased.

If the existence of oscillator-like behavior of the strongly unstable system is now well established, the relevant mechanism allowing the sustainment of oscillations is yet controversial, especially for bluff body wakes. The problem may be schematically formulated as identifying the feedback loop in space giving rise to the self-sustained oscillator. If the moving ''downstream'' branch of the loop is similar between all the models and is made of a vortical instability wave, the ''upstream'' branch closing the loop differs from one model to another.

One of the proposed mechanisms for wakes relies on hydroacoustic resonances (edge tones, wake tones) occurring when there is a second blunt body at a finite distance

downstream.[11] A feedback loop dominates the dynamics of the flow with a downstream branch consisting of rotational instability waves rolling up into vortices and an upstream branch consisting of irrotational pressure disturbances generated by interaction between the vortical structures and the downstream body. The pressure perturbation is converted into vortical instability mode at the separation point. This mechanism might also apply when no downstream body is present, the pressure wave being directly emitted by the growing and saturating vortices.[11] Precise threshold value or scaling laws generic to the class of self-sustained resonance we consider have not been predicted using this mechanism.

An original mechanism has been proposed by Villermaux[12] in the form of a nonlinear delayed feedback which models the reintroduction of disturbances close to the bluff body by the counter flow which exists just behind the cylinder. This mechanism applies well to describe the low-frequency modulation of the large scale von Kármán vortices at high Reynolds numbers in an order-one aspect ratio container. This large-scale structure would originate in the low-frequency modulation on the small scale Kelvin–Helmholtz instability of the separated shear flow. However, this model is unable to explain the self-sustained resonance observed in hot jets, convection cells with throughflow or Taylor–Couette rolls with an added Poiseuille flow in which no recirculation is present. In the case of the cylinder wake, this model fails to predict the bifurcation structure at low Reynolds numbers.

Another proposed mechanism is concerned with a feedback loop closed by a decaying vortical instability wave[13] moving upstream, and has been associated with the notion of absolute instability.[14–16] This concept refers to the behavior of the impulse response of the parallel flow obtained by extending to infinity the flow that exists at a particular station x (the so-called local instability). If localized disturbances spread upstream and downstream and contaminate the entire flow, the system is said to be *absolutely unstable*. If, in

contrast, disturbances are swept away from the source, the system is said to be *convectively unstable*. Using the notions of local absolute and convective instability, most open shear flows have been recently investigated and the existence of a global mode has been associated with local linear instability of the flow (see Ref. 1 for a review). The term ''global mode'' usually refers to the exponentially growing in time solution of a nonhomogeneous linear eigenproblem involving the whole streamwise direction, and the ''global instability'' refers to its existence. The connection between global instability and local absolute nature of the instability has been first established on model equations and subsequently extended to real flows.[17] In the weakly nonparallel approximation, a sufficiently large region where the instability is locally absolute has been shown to lead to an unstable global mode.[18] Bifurcation threshold predicted by this weakly nonparallel theory is well confirmed by direct numerical simulation in the case of the wake with added counter flow).[19]

In more complex geometry, all three feedback mechanisms might be active[20] and the ultimate goal will be to be able to precisely quantify each mechanism. However, at present, it seems likely from numerous experimental and numerical results[1] that the feedback through vortical instability wave that we will discuss does apply for the first bifurcation of wakes,[5] mixing layer with counterflow,[7] light jets,[6] and Rayleigh–Bénard[9] and Taylor–Couette flow[10] with throughflow.

If the linear global stability analysis is quite well established, it is not so for the effect of nonlinearity and a precise description of the bifurcation is lacking. In the present paper, we will consider fully nonlinear solutions of a model amplitude equation and compare directly results derived for these models to real experiments. However, we have to keep in mind that these flows are far from local threshold, and that the real flow dynamics does not reduce exactly to the model amplitude equation. Therefore, the comparison should be at best qualitative.

For model equations, it has been shown by Chomaz et al.[18,21] that a necessary condition for the linear global instability is the existence of a finite region of absolute instability. Once the linear global stability was solved and analyzed in the Wentzel–Kramers–Brillouin–Jeffrey (WKBJ) framework,[22] it was natural to study the weakly nonlinear behavior[23] as early experimental evidence[5] shows that the global bifurcation was following the Landau equation. Unfortunately, the weakly nonlinear problem turns out to be ill posed in the sense that the approach is valid only when the departure from threshold is exponentially small in comparison with the inhomogeneity parameter.[24] This drastic limitation of the ''easy nonlinear theory''[25] may be explained by the fact that for order-one advection velocity, the second-order modification of the basic flow due to the growth of the perturbation occurs far downstream of the region determining the growth rate of the linear global instability. When small but not exponentially small departures from threshold are considered, a fully nonlinear study is necessary and is the aim of the present paper.

In previous studies,[26–31] we have carried out a fully nonlinear study of a homogeneous flow for potential and nonpotential cases.[29,30] This homogeneous model[29,30] predicts the occurrence of a self-sustained nonlinear solution when a front is able to sustain the advection. This solution is derived from the front solution obtained by Kolmogorov et al.[32] in the potential case and by Dee[33,34] in the nonpotential case, and occurs for the Ginzburg–Landau equation at the precise value where the flow goes from convective to absolute instability. Indeed, it has been shown in Ref. 35 that the selection of the fully nonlinear front solution occurs through the linear ''marginal stability criterion.'' The front impinging on the boundary condition allows us to predict the scaling law at the global bifurcation. The models gives a good agreement with the numerical observations by Büchel et al.[10] for the Taylor–Couette problem with throughflow, or by Müller et al.[8,9] for the Rayleigh–Bénard problem with an added Poiseuille flow.

We will present here extensions of these previous studies to the inhomogeneous case and we assume that the control parameter $\mu(x)$ varies linearly in x, the direction of the flow. This assumption does not restrict the generality of the study since the method could be applied to arbitrary $\mu(x)$. Moreover, we focus this study on the case of a real amplitude equation for the sake of simplicity since, as for the homogeneous case, the nonhomogeneous global mode has a similar structure for the real and complex amplitude.[28,29]

We present the model in Sec. II. We assume that nonlinearities dominate inhomogeneity and we make a weakly non parallel assumption, using a small parameter μ_1 accounting for the inhomogeneity of the medium, $(\mu(x) = \mu_0 - \mu_1 x)$. In the case of an order-one advection velocity, this hypothesis allows us to derive in Sec. III, a matched solution exactly representing the saturated weakly nonparallel global mode with the upstream boundary condition that the amplitude of the perturbation is zero at $x = 0$. In Sec. IV, we derive scaling laws for the maximum amplitude of the global mode and its position versus the departure from instability threshold. In Sec. VI, the analytical solution and the scaling laws found in Sec. IV allow a direct and quantitative comparison with the experimental results by Goujon-Durand et al.[2] and with the numerical results by Zielinska and Wesfreid[3] which concern the wake of angular obstacles. They observe the variations of the amplitude of the longitudinal velocity component in the streamwise direction similar to those obtained in our model. According to these observations, the nonlinear saturation of the amplitude occurs on a smaller scale than the scale of streamwise variation of the mean flow, allowing our weakly nonparallel assumption to be correct at leading order. A discussion of this hypothesis is done in Sec. VI. The scaling laws for the maximum amplitude and its position versus the departure from instability threshold predicted by the present theoretical approach are in good agreement with those observed by these authors.

II. THE GINZBURG–LANDAU MODEL

Ginzburg–Landau equations describe the evolution of the amplitude of unstable modes for any process exhibiting a Hopf bifurcation, for which the continuous band of wave numbers is destabilized. More generally, Ginzburg–Landau equations are relevant to describe spatially extended systems

when oscillations or waves are present.[36] In the present paper, the Ginzburg–Landau model describes the evolution of the complex amplitude of instability waves which develop in the wake behind a cylinder. For simplicity, coefficients will be assumed real since a similar behavior is observed for complex coefficients. In a real flow, the laboratory frame is usually singled out by the conditions at the entrance of the flow; this breaks the Galilean invariance and leads us to take into account the mean advection velocity of the flow explicitly. Mixing layers[37] and wakes evolve in space. Therefore, inhomogeneity of the flow modifies the local stability characteristics and has to be taken into account explicitly. In the model, this inhomogeneity is introduced in the local growth rate $\mu(x)$ which varies in the streamwise direction and is assumed for simplicity to be such that the flow is stable at infinity, i.e., such that $\mu(+\infty)<0$. The objective of the present paper is to describe the spatial structure of nonlinear global modes of a nonparallel flow, which in the present case are steady fully nonlinear solutions of the real Ginzburg–Landau equation with varying coefficient $\mu(x)$ and with a nonzero advection term $U_0>0$:

$$\frac{\partial A}{\partial t}+U_0\frac{\partial A}{\partial x}=\frac{\partial^2 A}{\partial x^2}+\mu(x)A-A^3 \tag{1}$$

in a semi-infinite domain $[0,+\infty)$ with an "entrance" condition,

$$A(0)=0, \tag{2}$$

and an asymptotic behavior at $x=+\infty$ dictated by the fact that the system is stable at infinity with a single fixed point $A=0$:

$$A(+\infty)=0. \tag{3}$$

The control parameter μ is assumed to depend linearly on the space variable x,

$$\mu(x)=\mu_0-\mu_1 x, \tag{4}$$

where μ_0 and μ_1 are positive constants. The length scale $L=1/\mu_1$ characterizes the inhomogeneity. This choice of a linear dependence is similar to the one used in Refs. 18, 38, and 39 to study the linear global stability and models a flow that becomes stable far downstream. It allows us to give a concrete and quantitative example of nonparallel flow for which the coefficients will be deduced from the numerical study by Hammond and Redekopp,[40,19] but it does not restrict the generality of the study since the model remains valid as long as $\mu(x)$ is any decreasing function depending on x only through a slow space variable $X=\mu_1 x$, with $\mu_1 \ll 1$.

In weakly inhomogeneous media ($\mu_1\ll 1$), the existence of a finite region of absolute instability has been shown[18,23] to be a necessary condition for the linear global instability. For the model (1)–(4), the basic state $A=0$ is locally linearly unstable for $\mu(x)>0$, i.e., for $x<x_0\equiv\mu_0/\mu_1$. In order to obtain the linear global instability for this model, a sufficiently large region of absolute instability should be present within the unstable region bounded by x_0. The linear theory
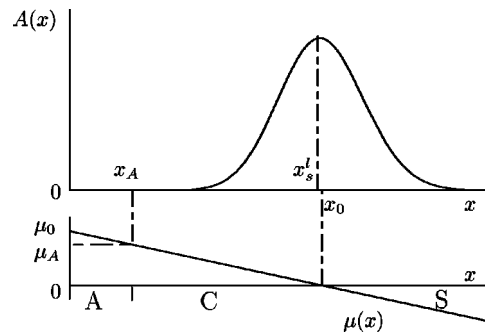

FIG. 1. Spatial structure of a linear global mode in the weakly nonlinear régime. x_s approaches x_0 (parameters in the W region in Fig. 4). The instability is locally absolute (A) near the origin and locally convective (C) between x_A and x_0. The system is stable (S) further downstream.

of absolute and convective instability[1] allows us to define the threshold μ_A of absolute instability as a function of the advection velocity:

$$\mu_A\equiv\frac{U_0^2}{4}. \tag{5}$$

Here, we consider U_0 of order one so that μ_A is also of order one. When $\mu(x)>\mu_A$, the basic state $A=0$ is locally absolutely unstable, i.e., locally linearly unstable with growing waves moving upstream and downstream and contaminating the entire medium. At the origin of the semi-infinite domain, we assume that the control parameter is greater than μ_A: $\mu_0=\mu_A+\epsilon$ ($\epsilon>0$), therefore, a finite region of absolute instability exists near the origin. This region of absolute instability is bounded by x_A, the distance at which $\mu(x_A)=\mu_A$:

$$x_A=\frac{\epsilon}{\mu_1}. \tag{6}$$

The size x_0 of the region of convective instability is such that $x_0\sim L$, since we consider μ_0 of order μ_A.

When the nonlinearity is weak compared to inhomogeneity as in the study by Le Dizès et al.,[24] the global mode may be described by a linear solution of Eq. (1) with the required boundary conditions:[41]

$$A(x)=e^{(U_0/2)x}\text{Ai}(\mu_1^{1/3}(x-x_A)). \tag{7}$$

Such a linear global mode has been shown to exist only when the control parameter μ_0 is larger than the linear threshold,

$$\mu_g^l=\mu_A+|\zeta_1||\mu_1|^{2/3}, \tag{8}$$

where ζ_1 is the first zero of the Airy function ($\zeta_1\simeq-2.338$). The position x_s^l of the maximum of the linear global mode (7) is simply determined by the root of the derivative of Eq. (7) and, when μ_1 goes to zero, it is found to scale like the inhomogeneity length scale L (when $\mu_1\ll 1$, we obtain $x_s^l\sim\mu_A/\mu_1\sim L$ since μ_A is of order one). A shape of the global mode typical for this exact result $x_s^l\sim L$ is sketched in Fig. 1.

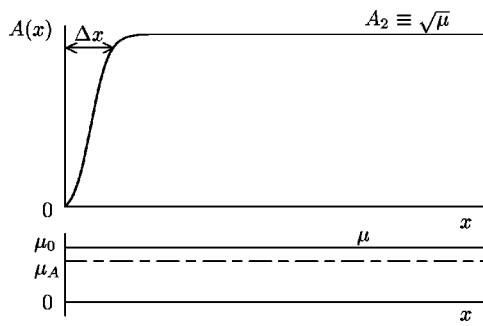Linear global modes bifurcate when the control parameter μ_0 exceeds the threshold of absolute instability by a

FIG. 2. Spatial structure of a homogeneous nonlinear global mode. The control parameter is constant $\mu(x)=\mu_0>\mu_A$. Δx is the distance at which the solution saturates.
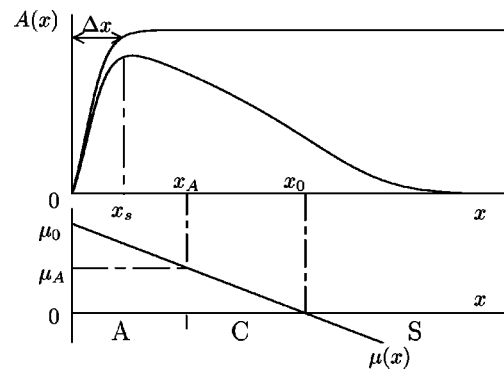

FIG. 3. Comparison of a NG mode with its homogeneous counterpart in the strongly nonlinear régime. Δx is smaller than x_A (parameters in the K region in Fig. 4). See caption of Fig. 1 for the meaning of A, C, and S.

quantity scaling like $\mu_1^{2/3}$. Le Dizès et al.[24] have shown that the weakly nonlinear theory is valid only when the departure from threshold $\mu_0-\mu_g^l$ remains smaller than an exponentially small quantity $[\mu_0-\mu_g^l<\exp(-1/\mu_1)]$, and, therefore, a fully nonlinear theory is necessary for larger departures from threshold.

For model (1) we have established in Ref. 28 the existence of fully nonlinear global modes in homogeneous media, i.e., when $\mu_1=0$ (parallel flow case). We know from Ref. 28 the spatial structure of steady solutions of (1) vanishing at the origin and saturating at a finite amplitude when $x\rightarrow +\infty$. In order to avoid confusion, these solutions for which the control parameter μ does not vary with respect to x will be denoted ''homogeneous'' nonlinear global (HNG) modes throughout the study. Please note that they are asymptotic to $A_2=\sqrt{\mu}$ at infinity. For Eq. (1), HNG modes exist only if the instability is absolute ($\mu>\mu_A$). In this case, the linear absolute/convective transition and the nonlinear global instability are simultaneous. In Ref. 28, we have defined the characteristic growth length of HNG modes as the distance at which the solution reaches 99% of its maximum amplitude A_2, and we have determined the scaling of Δx as a function of the departure from global instability threshold $\epsilon=\mu-\mu_A$, which has been shown to be such that

$$\Delta x \simeq \frac{1}{\sqrt{\epsilon}}. \qquad (9)$$

The typical spatial structure of HNG modes is sketched in Fig. 2 and corresponds to a front blocked on the upstream boundary condition.

In many ways, Δx may be considered as the correlation length scale of a flow with mean advection; its physics is a little more complex than the usual correlation length scale since it involves not only instability and diffusion, but also the advection.

The lengths L, x_0, x_A, and Δx are separately associated to particular physical effects which may be dominant depending on the relative value of the two small parameters ϵ and μ_1.

The problem faced here is the nonuniform limit $\mu_1\rightarrow 0$ and $\epsilon\rightarrow 0$ which imposes to define the range of variation for μ_1 compared to ϵ. Therefore, throughout this study, we will not only use a weakly nonparallel hypothesis ($\mu_1\ll 1$), but

also a stronger condition ensuring that nonlinearity dominates over nonparallelism in a sense that will be rigorously defined through the matching but that we are going to make precise with physical arguments.

Let us denote by x_s the position of the maximum amplitude of the NG mode (see Fig. 3). Actually, the scaling for x_s is unknown (except in the weakly nonlinear case where $x_s=x_s^l$). To estimate the conjugated effect of nonlinearity, instability, and advection in terms of a single length scale is, in general, not easy, but, in the present case, we chose the length scale Δx, taking advantage that Δx depends only on ϵ whereas x_s depends, in general, also on μ_1. It will turn out that the second length scale to consider will be x_A, which characterizes both the nonparallelism and the departure from threshold.

When $\Delta x\ll x_A$, nonlinear effects dominate over inhomogeneity. The solution initially (in space) grows as if the flow was homogeneous and reaches saturation once the basic flow is still absolutely unstable. Then, i.e., for $x>\Delta x$, it follows adiabatically the saturated amplitude $A_2=\sqrt{\mu(x)}$ until $\mu(x)=0$, where the flow will be stable and the amplitude almost zero. This typical spatial evolution is reported on Fig. 3. In that case, x_s is almost Δx.

In contrast, when $x_A\ll\Delta x$, inhomogeneity effects are dominant over nonlinear effects and the HNG mode structure is lost since it would correspond to a front blocked on the upstream boundary condition which saturates in a region where the flow is convectively unstable and, therefore, which would be washed out by the mean advection. In that case, Δx is no longer an estimate of x_s. This case corresponds to the weakly nonlinear régime[24,23] for which the global mode may be described by the linear solution (7), but it is valid only if the control parameter μ_0 belongs to an extremely narrow band around the linear threshold μ_g^l. As the nonlinear global mode is spatially identical to the linear one, the scaling of x_s should still be of the order of magnitude of L, the inhomogeneity length scale.

In conclusion, whether Δx is smaller or larger than x_A leads us to distinguish two regions of the parameter space (μ_1,ϵ). In the light gray region K in Fig. 4, ϵ is sufficiently large so as to allow the mode to grow and saturate within the locally absolute region $\Delta x\ll x_A$ [Fig. 3(b)]. The spatial grow-
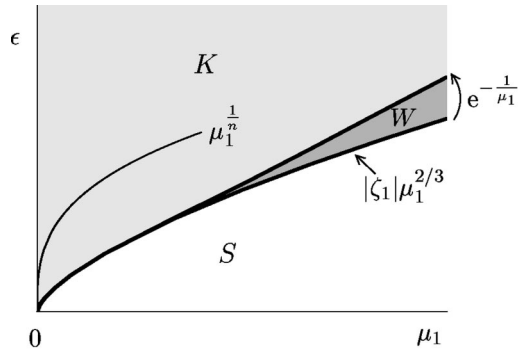
FIG. 4. Parameter space (μ_1, ϵ). The light gray region K indicates where the present fully nonlinear and weakly inhomogeneous description applies and the maximum amplitude position x_s of NG modes scales like the growth length $\Delta x \simeq \epsilon^{-1/2}$ of homogeneous NG modes (Figs. 2 and 3). In the dark gray region W, the weakly nonlinear theory on linear global modes (7) described by a WKBJ approximation (Ref. 24) is valid and x_s scales like L.
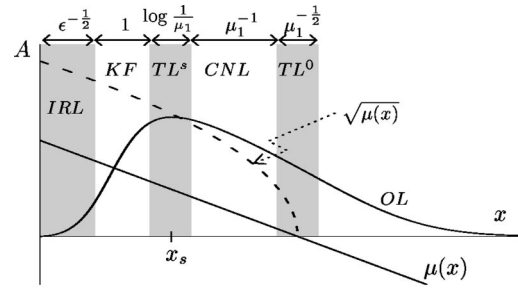

FIG. 5. Asymptotic solution of (1)–(3). The control parameter $\mu(x)$ is represented by the straight line. In the original semi-infinite domain, three transition layers [the inner resonant layer IRL at the origin, TL^s around the maximum amplitude and TL^0 near the point x_0 where $\mu(x_0)=0$] allow connection of the linear and nonlinear regions; as in Ref. 43, CNL denotes central nonlinear regions and OL is an outer linear region.

ing part of the NG mode will be identical to the one of a HNG mode if condition (10) is satisfied:

$$\Delta x \ll x_A \Leftrightarrow \frac{1}{\sqrt{\epsilon}} \ll \frac{\epsilon}{\mu_1} \Rightarrow \epsilon \gg \mu_1^{2/3}. \tag{10}$$

This naive thought is fully confirmed by the analysis in Sec. III where we will see that in the light gray K region in Fig. 4, i.e., when $\epsilon \gg \mu_1^{2/3}$, the spatial structure of the NG mode is at first order, the one of the Kolmogorov et al. front[32] which describes the HNG mode at leading order, and the next order which has to be taken into account as long as the solution grows in space is the departure from global instability threshold $\epsilon = \mu_0 - \mu_A$, and not the inhomogeneity which acts further downstream.

Inhomogeneity of the medium does not affect the position of the maximum amplitude which scales as $\epsilon^{-1/2}$ like the growth length of a HNG mode given by Eq. (9). This remains true when decreasing ϵ until the maximum amplitude x_s leaves the absolute region $x_s > x_A$.

The weakly nonlinear theory then applies to the linear global mode (7) in an exponentially small region (W) represented in dark gray in Fig. 4. A sharp variation of x_s occurs in this narrow band (dark gray region W in Fig. 4) for which $\epsilon - |\zeta_1|\mu_1^{2/3} \sim \exp(-1/\mu_1)$, and the NG mode shape jumps from the weakly nonlinear to the strongly nonlinear description.

In order to cover the gray region K above the $\epsilon = |\zeta_1|\mu_1^{2/3}$ line in (ϵ, μ_1) space (Fig. 4), the inhomogeneity parameter and the departure from global instability threshold ϵ are assumed to be connected by the relation

$$\mu_1 = \epsilon^n \tag{11}$$

with $n > \frac{3}{2}$, i.e., the set of continuous lines given by relation (11) $\epsilon = \mu_1^{1/n}$ with $n > \frac{3}{2}$ in Fig. 4 covers all of region K in light gray, and only one example has been drawn to illustrate. Our goal is to obtain a uniform convergence in μ_1 and ϵ in the light gray region K and to describe the spatial structure of NG modes in this region.

III. SPATIAL STRUCTURE OF NG MODES

Figure 5 represents an example of a NG mode obtained by numerical simulation of the evolution equation (1) with boundary conditions (2) and (3). Initially, the system is in the uniform state $A=0$ and an infinitely small (10^{-10}) perturbation is added at some location ($x=x_0/2$). The amplitude grows, saturates, and reaches a steady state. This asymptotic solution is a NG mode which satisfies the steady version of Eq. (1):

$$\frac{d^2A}{dx^2} - U_0 \frac{dA}{dx} + (\mu_0 - \mu_1 x)A - A^3 = 0, \tag{12}$$

with vanishing amplitude at the origin and at infinity. The spatial structure of the NG modes will be described theoretically using the method of matched asymptotic expansions[42] and is closely related to the structure of similar modes obtained in the case of doubly infinite domains.[43] We have to distinguish six subdomains in the original semi-infinite domain represented on Fig. 5.

The solution varies rapidly in the two first domains whereas it varies slowly (on a length scale $X = \mu_1 x$) in the remaining layers. The two first layers therefore have a structure very similar (but not identical) to the structure of the HNG mode described in Ref. 28, i.e., a Kolmogorov front impinging on the boundary. They are better described at leading order in the phase space $(A, dA/dx)$ since variations of the coefficients with x are slow. The other layers may be described in the WKBJ approximation.

The three main layers (KF, CNL, OL) are connected through two small transition layers (TL^s, TL^0) and connected to the boundary by an inner resonant linear layer (IRL), which may be viewed as the physical oscillator inducing the whole global mode structure.

The detailed structure of the NG mode represented in Fig. 5 will be described for each layer in the Appendix. In the following, we indicate only briefly the nature of the solutions in each layer and we focus on the description of the NG mode in the transition layer IRL which is the key layer for this matching. Indeed, the matching between this layer and KF determines the dominant part in the scaling law for the position of the maximum amplitude x_s, which will be
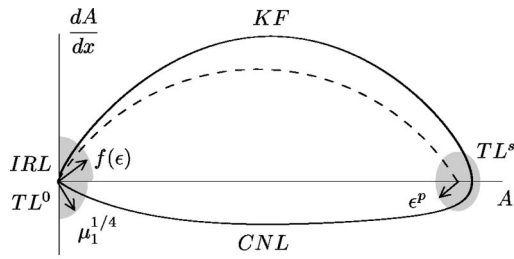
FIG. 6. The projection of the phase space in the plane $(A, dA/dx)$ shows the different layers (the transition layers being in gray). IRL [of size $f(\epsilon)$ given in Eq. (19)] and TL^s (of size ϵ^p) allow respectively satisfaction of the boundary condition at the origin and the connection in the phase space of the solution in CNL to the point of maximum amplitude. The decreasing part of the NG mode ($dA/dx < 0$) is close to the (A, x) plane of phase space and the matching of this part of the trajectory is then done in the physical space.

compared with experimental and numerical results for wakes by Goujon–Durand et al.[2] and Zielinska and Wesfreid[3] in Sec. VI.

A. Qualitative description of NG modes

1. Spatial structure of NG modes in the inner resonant layer IRL

The inner resonant layer IRL is crucial since the particular form of the solution in this layer allows us to respect the boundary condition by the beating of two waves. The matching will then be possible only for $\epsilon > 0$. For $\epsilon < 0$, the boundary condition at $x=0$ and the matching condition at the downstream boundary of IRL cannot be satisfied simultaneously.

In this layer, the amplitude is small since A vanishes at $x=0$. Denoting ξ the inner variable which is connected to the amplitude by the relation $A = f(\epsilon)\xi$, where the gauge $f(\epsilon) \to 0$ as $\epsilon \to 0$, ξ satisfies the linearized Eq. (12) around $A=0$:

$$\xi'' - U_0 \xi' + \mu(x)\xi = 0. \tag{13}$$

Since $\xi(x)$ must vanish at the origin, the solution of Eq. (13) may be written with one undetermined integration constant v_0 and using Airy functions,[44]

$$\xi(x) = \frac{v_0 \pi}{\mu_1^{1/3}} e^{(U_0/2)x} (a\mathrm{Bi}[(x-x_A)\mu_1^{(1/3)}]$$
$$- b\mathrm{Ai}[(x-x_A)\mu_1^{(1/3)}]), \tag{14}$$

where $x_A = \epsilon/\mu_1$ denotes as previously the size of the absolute domain, $a = \mathrm{Ai}(-x_A \mu_1^{1/3})$, and $b = \mathrm{Bi}(-x_A \mu_1^{1/3})$. The slope v_0 at the origin of the inner solution (14) will be fixed by the matching.

2. The Kolmogorov front layer

The phase space $(A, dA/dx)$ has to be used in order to represent the solution matching in the Kolmogorov front layer where the variations of A are fast. Figure 5 may be thought of as the projection in the plane (A, x) of the three-dimensional trajectory representing the NG mode in the phase space $(A, dA/dx, x)$, whereas Fig. 6 presents the same trajectory but projected on the plane $(A, dA/dx)$.

The different scales on Figs. 5 and 6 show that from x_s to $+\infty$ in the decreasing part of the trajectory, the NG mode evolves slowly; therefore, dA/dx keeps being small and the trajectory lays nearly in the (A, x) plane of the phase space and the slow variable $X = \mu_1 x$ could have been used to present this part of the trajectory. However, when considering the growing part of the NG mode ($x < x_s$), since $x_s \ll \mu_1^{-1}$ by assumption, x does not vary much on the scale μ_1^{-1} and the trajectory in the phase space is now close to the plane $(A, dA/dx)$, close meaning that the distance from the plane $(A, dA/dx)$ is small when measured in $X = \mu_1 x$ variable. The solution in KF then takes the form of a front linking a small amplitude to $\sqrt{\mu_A}$, which is reminiscent of the shape of a homogeneous NG mode[28] in the parallel flow case, described in the phase space $(A, dA/dx)$ as the stable manifold of a fixed point $(A_2, 0)$. This stable manifold is itself viewed as the perturbation of an heteroclinic trajectory linking the origin $(0,0)$ of phase space to the point $(A_2 = \sqrt{\mu_A}, 0)$ and representing the Kolmogorov front solution in an infinite homogeneous domain, presented in dashed line in Fig. 6 (see Ref. 28 for details). When $\mu = \mu_A + \epsilon$, the perturbed trajectory defines a homogeneous NG mode which links in the phase space, a point of the dA/dx axis to $(A_2, 0)$. When considering the effect of inhomogeneity, we must take into account a new perturbation in this trajectory by introducing corrective terms in μ_1 and $\mu_1 x$ in the basic front solution at threshold.

In the three-dimensional phase space $(A, dA/dx, x)$, the solution in KF is described as a series expansion of dA/dx in A with coefficients depending on x:

$$u(A) = \frac{dA}{dx} = \sum_{j=0}^{+\infty} (-\nu_j - \epsilon\lambda_j + \mu_1(\zeta_j + \eta_j x))$$
$$\times (A_2 - A)^j, \tag{15}$$

where ν_j, λ_j, ξ_j, and η_j are constant. Terms of order ϵ are by assumption larger than terms in $\mu_1 x$, since, in the KF layer, $x \lesssim \Delta x$ and, in the light gray region of Fig. 4, $\Delta x \ll x_A = \epsilon/\mu_1$. The matching between KF and TL^s [done in the phase space $(A, dA/dx, x)$] determines the first coefficients in the series (15), allowing us to compute other coefficients recursively. In practice, the coefficients expressed as an analytical formula have to be computed numerically. Note that when this matching is done, we obtain the result that x_s must be at least greater than the size $\log(1/\mu_1)$ of TL^s. After having computed the set of coefficients in Eq. (15), we know the asymptotic behavior of $u(A)$ when $A \to 0$:

$$u(A) \simeq -\sum_{j=1}^{+\infty} \nu_j A_2^j + \sum_{j=1}^{+\infty} j\nu_j A_2^{j-1}A + \mu_1 x \sum_{j=0}^{+\infty} \eta_j A_2^j$$
$$- \epsilon \sum_{j=0}^{+\infty} \lambda_j A_2^j + \mu_1 \sum_{j=0}^{+\infty} \zeta_j A_2^j. \tag{16}$$

We now proceed to the detailed description of the matching between IRL and KF.

3. Matching IRL→KF in the case $\mu_1 \ll \epsilon^{3/2}$

In the case $\mu_1 \ll \epsilon^{3/2}$ ($\mu_1 = \epsilon^n$ with $n > \frac{3}{2}$ in the light gray region in Fig. 4), we obtain $x_A \mu_1^{1/3} = \mu_1^{1/n - 2/3} \to +\infty$. Keeping in mind the condition $\mu_1 \ll \epsilon^{3/2}$ implies, the NG mode must reach its maximum inside the absolute domain ($x_s \ll x_A$), we may let x go to infinity in IRL by keeping the condition $x \ll x_A$ satisfied, and we obtain $(x - x_A)\mu_1^{1/3} \to -\infty$. Airy functions may be expanded using their asymptotic behavior at $-\infty$. We find again the inner solution already found for homogeneous global modes[28]

$$\xi(x) = \frac{v_0}{\sqrt{\epsilon}} e^{(U_0/2)x} \sin(\sqrt{\epsilon}x). \tag{17}$$

Order ϵ must be lower than order $\mu_1 x$ for all $x \ll x_A$, whatever the scaling law for the position of the maximum amplitude. The matching may then proceed with the same scaling laws than for homogeneous NG modes. As $x \to \pi\epsilon^{-1/2}$, solution (17) admits in the phase space the asymptotic behavior:

$$\frac{d\xi}{dx} \simeq \frac{U_0}{2}\xi - v_0 e^{(U_0/2)\,(\pi/\sqrt{\epsilon})}. \tag{18}$$

($\Delta x \simeq \pi\epsilon^{-1/2}$ is the characteristic growth length of homogeneous NG modes.) Replacing ξ by $A/f(\epsilon)$ in the inner expansion (18) and identifying with the expansion (16) in KL leads to the choice of the size of IRL [in the phase space $(A, dA/dx)$]:

$$f(\epsilon) = \epsilon e^{-(U_0/2)\,(\pi/\sqrt{\epsilon})}, \tag{19}$$

and to the following matching conditions:

$$\sum_{j=1}^{+\infty} \nu_j A_2^j = 0, \quad \sum_{j=1}^{+\infty} j\nu_j A_2^{j-1} = \frac{U_0}{2}, \quad \sum_{j=0}^{+\infty} \lambda_j A_2^j = v_0. \tag{20}$$

Terms in $\mu_1 x$ (and μ_1) do not have to be matched since the whole matching is done at leading order, and, as expected, the spatial structure of NG modes is fully consistent with the one of homogeneous NG modes.

From now on, matchings will be realized in the physical space as the variations in OL, TL^0, CNL, and TL^s are slow.

4. The central part

In the central nonlinear layer (CNL) of size μ_1^{-1}, the amplitude of the solution is saturated; it follows adiabatically the variation of μ. The amplitude in CNL is at first order the weakly decreasing function $A \sim \sqrt{\mu_0 - \mu_1 x} = \sqrt{\mu(x)}$, for which the slope remains small at each station. It reflects the interplay of nonlinearities and inhomogeneity and can be formulated as the nonlinear WKBJ solution of the problem. It decreases slowly from its maximum at x_s to a small amplitude ($\sim \mu_1^{1/4}$) at which the solution must be matched with the linear outer solution of Eq. (12) in OL, via TL^0.

At the upstream boundary of CNL, the amplitude is close to its maximum value. Since we assume that the distance from the origin to x_s, the position of the maximum amplitude, is much smaller than μ_1^{-1}, the maximum amplitude is at first order $\sqrt{\mu_0} \simeq \sqrt{\mu_A}$. In the transition layer TL^s

around x_s, the amplitude is then a linear solution of Eq. (12) linearized around $A = \sqrt{\mu_A}$. Since Eq. (12) is of second order, we must determine two integration constants. One is given by the matching with the solution in CNL, and the condition that x_s realizes a maximum of the amplitude yields the second one.

5. The downstream part: Matching CNL to OL via TL^0

In OL, the flow is strongly linearly stable; nonlinear terms in Eq. (12) are neglected and the solution reflects the interplay of advection and inhomogeneity as the product of a shifted Airy decreasing function with an exponential term (due to the advection) [see Eq. (A21)]. It may be also viewed as the linear WKBJ solution which follows adiabatically the variation of the linear wave number.

In the transition layer TL^0 of size $\mu_1^{-1/2}$, the basic state is nearly neutral; nonlinearities, advection, and inhomogeneity possess the same order of magnitude ($\sim \mu_1^{1/4}$) in Eq. (12) and the corresponding solution matches both solutions in CNL and OL. At this stage, note that the matching in TL^0 fixes the position of the layer TL^0 around the point x_0, but does not give any information about the position of the maximum x_s (which is two layers away).

Our analysis describing a NG mode in a weakly inhomogeneous medium as a perturbed front solution is therefore only valid when $\mu_1 \ll \epsilon^{3/2}$ in the light gray K region in Fig. 4. The conclusion of this section is that, in Fig. 4, we have extended the weakly nonlinear theory for NG modes, valid in the dark gray W region, to a strongly nonlinear theory which applies in the light gray region. In the light gray region K, inhomogeneity modifies only the tail of the homogeneous nonlinear global mode and not its front shape near the boundary. In the dark gray region W, the conjugated effects of inhomogeneity and advection acts strongly on the growing part as on the tail of the NG mode: if the growing part were described at leading order by a front at a position greater than x_A, it would experience a convective instability and would be advected downstream. While being advected downstream, the maximum amplitude decreases till weakly nonlinear effects are able to counterbalance inhomogeneity and advection. Then the solution finds equilibrium near the position x_0 where the flow becomes stable again.

IV. SCALING LAWS FOR x_S AND FOR THE MAXIMUM AMPLITUDE

The matching has been shown to be possible when $\mu_1 \ll \epsilon^{3/2}$. We now proceed to the description of the scaling laws directly given by the matching for the maximum amplitude and its position.

In the transition layer IRL, the solution grows until the inner amplitude becomes of order one, i.e., on a distance which scales like $\epsilon^{-1/2}$. In the Kolmogorov front region KF, the NG mode keeps growing until $A = A_2 - \epsilon^p$ (or until the upstream part of TL^s where the rescaled inner amplitude is of order one; see the Appendix, Sec. 2). The contribution of this layer TL^s in which the solution saturates to the characteristic growth length scales like $\log(1/\epsilon)$ [or equivalently $\log(1/\mu_1)$ because of the exponential dependence of the amplitude [see

Eq. (A9)]. Thus, the total growth length is determined at the lowest order solely by the inner resonant layer and reads

$$x_s \simeq \frac{\pi}{\sqrt{\epsilon}} \quad (\text{when } \mu_1 \ll \epsilon^{3/2}), \quad \text{i.e.,} \quad x_s \simeq \Delta x \ll x_A \ll L.$$
(21)

At this stage, it should be noted that the specific form of the control parameter profile far behind the leading edge does not influence the scaling law for x_s which coincides at lowest order with the scaling found for the length of a HNG mode. While the latter scaling does not depend on μ_1, there is nothing to prevent the variation of $\mu(x)$ from causing second-order distortions in x_s. The same remark is valid for the maximum amplitude as will be shown below. The maximum amplitude is reached in TL^s. The detailed structure of the NG mode in this layer is given in the Appendix, Sec. 2 as a small correction to the saturation amplitude $A_2 \equiv \sqrt{\mu_A}$ of homogeneous NG modes. From Eq. (A11), we obtain immediately the maximum amplitude of the global modes which reads

$$A_s \simeq \sqrt{\mu_A} + \epsilon \frac{1}{2\sqrt{\mu_A}} - \frac{\mu_1}{\sqrt{\epsilon}} \frac{\pi}{2\sqrt{\mu_A}} \quad (\text{when } \mu_1 \ll \epsilon^{3/2}).$$
(22)

The maximum amplitude is only slightly modified with regard to the maximum amplitude $\sqrt{\mu_A + \epsilon}$ valid for HNG modes. This is not surprising since our fully nonlinear hypothesis implies that we have to remain sufficiently far from threshold in order for the inhomogeneity to act as a perturbation on the homogeneous fully nonlinear case. Moreover, Eq. (22) is fully consistent with the extrapolation:

$$A_s \sim A_2(x_s) \simeq \sqrt{\mu_0 - \mu_1 x_s} \simeq \sqrt{\mu_A} + \frac{1}{2\sqrt{\mu_A}}(\epsilon - \mu_1 x_s),$$
(23)

and introduction of (21) into expansion of (23) in powers of ϵ yields exactly Eq. (22).

V. NUMERICAL VALIDATION OF THE SCALING LAWS

To test the validity of the model, we have compared the scaling law (22) with results from numerical temporal simulations using a realistic value of the inhomogeneity parameter $\mu_1 = 0.01$ which has been deduced as will be seen below from the work of Hammond and Redekopp.[40,19] Figure 7 shows the values of the maximum amplitude and its position as a function of the ratio of the control parameter to the threshold value μ_0 / μ_A. The dots are computed using temporal simulations by the very long time behavior (up to a million time steps) of the real system (1) with 1500 points spaced by 0.1. The time marching is implicit, allowing a great deal of efficiency. We have also reported by a vertical axis the value of the shift on the linear global threshold ($\mu_g^l = \mu_A - \zeta_1 \mu_1^{2/3}$, where $\zeta_1 = -2.338$ is the first zero of the Airy function) derived by Chomaz $et\ al.$[18] using the linear theory. This threshold may be approached by the numerical data with less than 0.4% error.
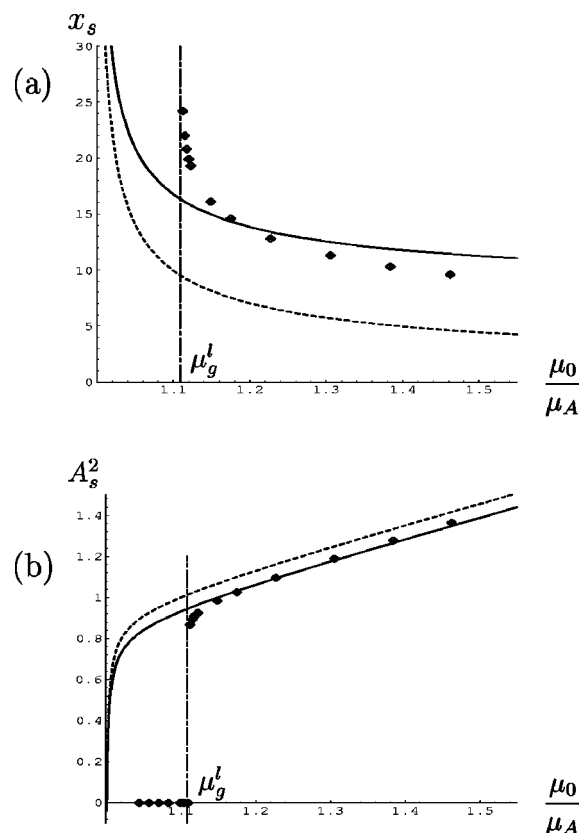

FIG. 7. (a) Comparison of the position of the maximum amplitude obtained by numerical simulation of the evolution equation (1) (dots) with the scaling law (21) (dashed line). The continuous line represents (21) with a second-order contribution to x_s in $\log(1/\mu_1)$. (b) Same as (a) with numerical data for the maximum amplitude compared to (22). We have used the value $\mu_1 = 0.01$ estimated from Refs. 40 and 19. The interrupted line indicates the weakly nonlinear Landau theory with a Landau constant of 10^{-22}. It crosses the axis at the linear global threshold μ_g^l computed in Ref. 18 with respect to the local absolute threshold. When $\mu < \mu_g^l$, we have obtained that the flow relaxes to zero following the linear global mode theory (Ref. 18) with $A_s = 0$, but $x_s = x_g^l \sim 106$ here.

Since the present theory is valid in the strongly nonlinear regime $\epsilon \gg -\zeta_1 \mu_1^{2/3}$, the parts of the curves on the left of the linear threshold μ_g^l are not relevant. On the right of μ_g^l, we obtain a good qualitative agreement between the scaling law (21) [dashed line in Fig. 7(a)] and the numerical results obtained for the position of the maximum amplitude (dots), which becomes more quantitative when the nonparallelism μ_1 approaches zero (data not shown). The continuous line represents the scaling law (21) with addition of the second-order contribution to x_s in $\log(1/\mu_1)$ computed from Eq. (A9). The scaling law (22) for the maximum amplitude [dashed line in Fig. 7(b)] is very close to the obtained numerical values and, when using the second-order contribution in $\log(1/\mu_1)$ to x_s, the agreement is even closer (continuous line). Therefore, the results reported in Fig. 7 show that scaling (21) and (22), derived theoretically using the uniform limits as ϵ and μ_1 simultaneously tends to zero, describe with good agreement the numerical solution obtained by integration of (1) using a fixed (small) value of μ_1, except in a small range above the linear global threshold. In this range simulations need a large number of time steps to

reach equilibrium and, therefore, the size of this range is difficult to quantify, but, for the value of inhomogeneity parameter used, it is less than 0.4 % and decreases when using smaller values of μ_1. For this relatively small value of μ_1, the agreement of the computed location of the maximum x_s and the scaling law (in interrupted line), $x_s \simeq \epsilon^{-1/2}$ is at leading order correct.

The Landau constant given by the weakly nonlinear Landau theory developed in Refs. 23 and 31 has been computed as

$$c = \frac{\langle A^\dagger(x) | A^3(x) \rangle}{\langle A^\dagger(x) | A(x) \rangle} \tag{24}$$

where $\langle | \rangle$ stands for the usual inner product over the interval $[0, +\infty)$. The quantity $A(x)$ is the linear global mode defined by Eq. (7), and $A^\dagger(x) \equiv e^{(-U_0/2)x} \mathrm{Ai}(\mu_1^{1/3}(x - x_A))$ belongs to the kernel of the adjoint operator at μ_A. The Landau constant then equals 10^{-22}. This extremely small value is represented by the interrupted line of slope 10^{-22} in Fig. 7(b) which indicates that a departure of 10^{-22} above the linear global threshold μ_g^l is sufficient to reach order-one amplitudes. This sharp transition predicted by the linear global mode theory is in agreement with the numerically obtained fast variation of A_s^2 with μ, shown in Fig. 7(b) close to μ_g^l.

VI. COMPARISON WITH EXPERIMENTAL AND NUMERICAL RESULTS IN WAKES

In Ref. 2, Goujon-Durand *et al.* have studied experimentally the evolution of the global mode issued from the destabilization of the wake behind a trapezoidal bluff body. They have measured the streamwise and the crosswise velocity on the axis and at one diameter off the axis for a large region of streamwise location. Repeating this measurement for several Reynolds numbers R (i.e., increasing the mean flow velocity), they have shown the existence of a universal curve for the renormalized amplitude of the streamwise velocity profile. They have rescaled the amplitude by its maximum value and the streamwise coordinate by the position of the maximum and they have found that the data collapse to a single curve [Fig. 8(a)]. They have proposed the following scaling laws for the maximum amplitude value A_s and position x_s, which fit their measurements:

$$A_s \simeq A_0 (R - R_c)^{1/2}, \tag{25}$$

$$x_s \simeq (R - R_c)^{-1/2}, \tag{26}$$

where $R - R_c$ denotes the departure from critical Reynolds number R_c for the occurrence of the global mode, R_c being experimentally determined by plotting A_s^2 versus R. In Ref. 3, Zielinska and Wesfreid have presented results from two-dimensional numerical simulations of wake flow behind a triangular obstacle and confirmed the experimental results of Goujon-Durand *et al.*[2] In particular, the form of global modes and their dependence on the Reynolds number found numerically were in agreement with the scaling laws (25) and (26) given in Ref. 2. The universality of these scaling laws is reinforced by the fact that a different body has been used in the two studies (triangular in Ref. 3 and trapezoidal

in Ref. 2). Only when the wake is confined by side boundaries at ± 5 diameters, the rescaled global mode shape appears to vary with R.

A. Comparison of the scaling laws

Direct comparison of those real two-dimensional flow dynamics with our oversimplified model might seem unrealistic, but the scenario and behavior obtained with our toy model applies amazingly well to the real world. It is well known that Ginzburg–Landau models are valid well beyond expectations for many instabilities; for example, for Rayleigh–Bénard convection or the Taylor–Couette flow, the dynamics is dominated by the unstable mode at threshold even far from threshold. The same unexplained validity of the Ginzburg–Landau model has been observed by Albarède and Monkewitz for the orientation of the vortices in the wake of a cylinder.[45] In the present case, a simplified version of the Ginzburg–Landau model gives the correct scaling laws, which indicates that the essential ingredients necessary to describe the physics of wakes have been kept in our model.

Indeed, it is quite remarkable that the theoretical [Eq. (21)] and experimental [Eq. (26)] laws for the location of the maximum x_s are identical. Comparison of the predicted and the observed scaling laws for the amplitude is less straightforward since the theory is the leading order of our asymptotic expansion, which links ϵ and μ_1, the departure from criticity and the nonparallelism parameter, whereas ϵ and μ_1 are finite in the experiment. To compare with (25), the theoretical scaling law for the maximum amplitude (22) should be extrapolated by considering that A_s is a function of the parameters ϵ and μ_1 which are no longer connected through the relation $\mu_1 = \epsilon^n$. In the expansion (22), we transform the sum $\sqrt{\mu_A} + \epsilon/2\sqrt{\mu_A}$ back into the unique term $\sqrt{\mu_0} = \sqrt{\mu_A + \epsilon}$. When μ_1 is kept constant and ϵ independently is brought to zero, Eq. (22) shows that A_s becomes negative and even singular. The value of ϵ at which this extrapolated scaling laws predict a zero maximum amplitude is obtained by $A_s(\epsilon_{3/2}) = 0$ when

$$\epsilon_{3/2} \simeq \frac{\pi^2}{4\mu_A^2} \mu_1^2 \quad (\text{for } \Delta x \ll x_A). \tag{27}$$

Keeping in mind that $\mu_1 \ll 1$, we find that $\epsilon_{3/2} \ll -\zeta_1 \mu_1^{2/3}$, i.e., the scaling law (22) should be valid as soon as the linear threshold μ_g^l is exceeded by an exponentially small quantity corresponding to the weakly nonlinear regime. Therefore,

$$A_s^2 \sim \mu_A + \epsilon - \mu_1 x_s, \tag{28}$$

with x_s given by Eq. (21) [which yields Eq. (22)] is extremely close to the scaling law (25) observed experimentally and numerically in Refs. 2–4.

Comparison between model and reality seems to be qualitatively extremely favorable since Eq. (26) is correctly predicted and Eq. (25) is predicted at leading order. To make the comparison quantitative, we still face the problem that the nonparallelism of the flow (measured in the model by μ_1) is finite and, far from critical, depends on the Reynolds number which itself defines the instability of the flow measured by ϵ in the model. Therefore, for the wake flow, μ_1

and ϵ are functions of a single control parameter R and the representative point corresponding to real experiment in the (μ_1, ϵ) plane (Fig. 4) moves on a curve parametrized by R for which ϵ will go to zero while μ_1 will stay finite at threshold. For large enough ϵ, the representative point $(\mu_1(R), \epsilon(R))$ will always enter increasing R the gray domain of Fig. 4 where the theory we have developed applies but only at leading order (i.e., when both μ_1 and ϵ go to zero). We shall therefore extrapolate the results we have theoretically derived to finite value of (μ_1, ϵ) using numerical simulation of (1) before comparison with experiments.

B. Comparison of the global mode profile

In order to show more clearly the quantitative agreement between the model (1) and the experimental observations by Goujon-Durand et al. and the numerical observations by Zielinska and Wesfreid,[3] we have integrated numerically the evolution equation (1). We follow to that aim the derivation of Monkewitz et al.[17] Model (1) is in scaled variables (the amplitude, the time, and the streamwise coordinate) such that the coefficients of the diffusive term and the coefficient of nonlinearity are unities; but if the model (1) had been derived from the full two-dimensional Navier–Stokes equations, using a weakly nonparallel assumption as in Ref. 17, the Ginzburg–Landau equation obtained would use dimensionless variables based on physical scales such as the size d of the body, the velocity U_∞ of the stream flow without body, and the time scale d/U_∞. Using these units based only on physical scales, the local linear dispersion relation of instability waves is a function of the Reynolds number and the dimensionless streamwise slow coordinate X, and may be written in the form

$$\omega = \omega_R(X, R) + \omega_k(X, R)k + \tfrac{1}{2}\omega_{kk}(X, R)k^2, \quad (29)$$

where $\omega_k \equiv \partial \omega / \partial k$ and $\omega_{kk} \equiv \partial^2 \omega / \partial k^2$. In this expansion, we have substracted the carrier wave of maximum linear growth rate. For convenience, the dispersion relation (29) may be recast in the form of a Taylor expansion around the wave number $k_0(X, R) \equiv -\omega_k(X, R)/\omega_{kk}(X, R)$, corresponding to a saddle point of the dispersion relation at X:

$$\omega = \omega_0(X, R) + \frac{\omega_{kk}(X, R)}{2}(k - k_0(X, R))^2, \quad (30)$$

where $\omega_0(X, R) \equiv \omega_R(X, R) - \omega_{kk}k_0^2/2$. This expansion represents the dispersion relation associated with the equation

$$\frac{\partial A}{\partial T} - \omega_{kk}(X, R)k_0 \frac{\partial A}{\partial X}$$

$$= i\frac{\omega_{kk}(X, R)}{2}\frac{\partial^2 A}{\partial X^2} - i\left(\omega_0(X, R) + \frac{\omega_{kk}(X, R)}{2}k_0^2\right)A, \quad (31)$$

in which terms coming directly from nonparallelism have been omitted (see Ref. 17). Note that the complex group velocity ω_k is equal to the term $\omega_{kk}k_0$. When including the leading-order nonlinear term compatible with translational invariance in time $|A|^2A$, and after expanding $\omega_0(X, R)$,

$\omega_{kk}(X, R)$, and $k_0(X, R)$ at first order in the variable X and assuming that $\omega_{kk}(X, R)$ and $k_0(X, R)$ dependence on X are acting at higher order, we obtain

$$\frac{\partial A}{\partial T} - \omega_{kk,0}(R)k_{0,0}(R)\frac{\partial A}{\partial X} = i\frac{\omega_{kk,0}(R)}{2}\frac{\partial^2 A}{\partial X^2} - \gamma|A|^2A$$

$$- i\left(\omega_{0,0}(R) + \frac{\omega_{kk,0}(R)}{2}k_{0,0}^2(R) - \left.\frac{d\omega_0}{dX}\right|_0 X\right)A. \quad (32)$$

This model needs the evaluation of the complex coefficients $\omega_{kk,0}(R)$, $\omega_{0,0}(R)$, $d\omega_0/dX|_0$, $k_{0,0}(R)$, and γ, where the second subscript, ''0'' indicates evaluation of the function at $X = 0$. Finally, we assume that only Im$[\omega_{0,0}(R)]$, which models the local growth rate of instability waves, depends on the Reynolds number and is proportional to R.

The coefficients of Eq. (32) may be all deduced from the work of Hammond and Redekopp,[40,19] except from the nonlinear coefficient γ. They study numerically the two-dimensional wake behind the rectangular based body and compute the local growth rate $\sigma(X) \equiv$ Im$[\omega_0(X, R)]$ as a function of the distance to the body. Their Fig. 6 in Ref. 40 and Fig. 13 in Ref. 19 exhibit a parabolic variation of $\sigma(X)$, in contrast with our assumption of a linear variation. Using the theoretical framework developed in Ref. 17 for an infinite domain, they have computed the complex coefficients of Eq. (32) for a criticity of 33%. The complex coefficients we will use are estimated from theirs. Because of their quadratic variation of Im(ω_0) in X, they do not obtain directly a value for d Im$(\omega_0)/dX|_0$, but a coefficient of the quadratic term (which equals 0.0149) that we are going to identify to d Im$(\omega_0)/dX|_0$, as we just need an order of magnitude. This value of μ_1 evaluated by the computation of the coefficients corresponds approximatively to the mean slope of $\sigma(X)$ determined by Hammond and Redekopp (Fig. 6 in Ref. 40 and Fig. 13 in Ref. 19). We might as well have chosen d Im$(\omega_0)/dX|_0 \sim \sqrt{d^2 \text{Im}(\omega_0)/dX^2}$ in order to identify the typical size of the nonparallel effect; this would have led to an order of magnitude larger μ_1 for which the difference is minor departures from the asymptotic laws (21) and (22) affecting a larger range in ϵ.

Let us first rewrite Eq. (32) by rescaling the streamwise coordinate X [using the change of variable $X = x\sqrt{-\text{Im}(\omega_{kk,0}/2)}$] in order to set the coefficient of the diffusive term to unity; the amplitude is also properly rescaled to eliminate the imaginary terms proportional to $\partial A/\partial x$ and A, and to set the real part of the nonlinear coefficient to unity. We obtain a complex version of Eq. (1):

$$\frac{\partial A}{\partial T} + U_0\frac{\partial A}{\partial x} = (1 + ic_1)\frac{\partial^2 A}{\partial x^2} + (\mu_A + \epsilon - \mu_1 x)A$$

$$- (1 - ic_3)|A|^2A, \quad (33)$$

where all coefficients are obtained from those of Eq. (A1) computed in Ref. 19 after applying the rescaling. Since the model (1) is real and since we use values of the coefficients obtained in Ref. 19 for a complex model, we therefore have a crude estimation which is sufficient since only the order of magnitude is necessary. The advection velocity is estimated
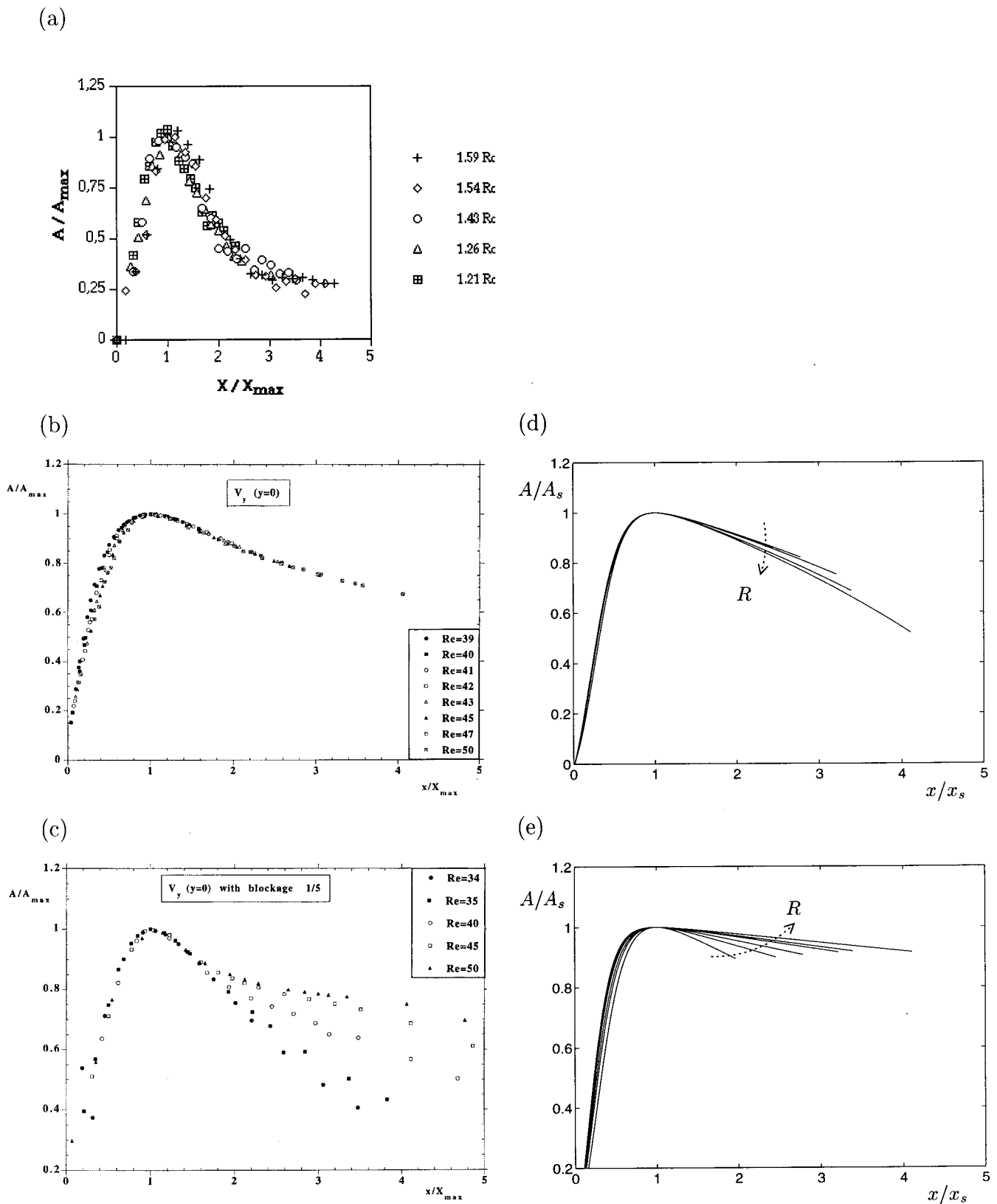
(a)

(b)

(d)

(c)

(e)

FIG. 8. Renormalized global modes scaled with A_s and x_s with the same departures from critical Reynolds number ($R_c \sim 38.3$) than in Ref. 3, corresponding to R=41, 42, 43, 45, 47, 50. (a) Experimental data for the NG mode associated with transversal velocity component of the wake from Ref. 2. (b) Numerical data from Ref. 3. (c) Numerical data from Ref. 3 with variation of the blockage. (d) Results of the present study for which the inhomogeneity parameter has been estimated for each ϵ from Fig. 3(b) in Ref. 3. (e) Results of the present study using a constant inhomogeneity parameter $\mu_1 = 0.033$ (no free parameter).

to $U_0 \simeq 2$ and its link to the threshold value μ_A [Eq. (5)] yields $\mu_A \simeq 1$. The inhomogeneity parameter is estimated to $\mu_1 \simeq 0.033$ as explained above.

Once μ_1 has been estimated, the model (1) then depends on the criticality $\epsilon = \mu_0 - \mu_A$. Typical criticalities ϵ are obtained using the same values of the ratio $(\mu_0 - \mu_g^l)/\mu_g^l$ as in experiment for the ratio $(R - R_c)/R_c$, leading to a comparable departure from instability threshold $\epsilon \equiv (R - R_c)/R_c$.

Experimental results obtained by Goujon-Durand *et al.*[1] for the NG modes associated with transversal velocity component of the wake are sketched in Fig. 8(a) for different values of the Reynolds number, after having renormalized the amplitudes to set A_s and x_s to unity. A unique shape is observed since the global modes are practically superposed into one curve for the different Reynolds number. Figure 8(b) presents the NG modes obtained numerically by Zielinska and Wesfreid[3] for unconfined wake, after renormalizing the amplitudes in the same way as in Fig. 8(a). The numerical data obtained for the different Reynolds numbers show that the renormalized NG modes are superposed into one curve exactly as for the experimental results by Goujon-Durand *et al.*[2] [Fig. 8(a)]. When the wake is laterally confined,[3] the numerically computed nonlinear global modes reported in Fig. 8(c) show that the growing parts of the NG modes are still superposed into one curve exactly but not the tails. Before discussing the results obtained in the present study with the protocol described above, let us remark that experimental or numerical data in Ref. 2 and 3 have been measured in a fixed short domain $[0, x_M]$. Therefore, the rescaled NG modes plotted in Fig. 8(a)–8(c) seem to be shorter (in the rescaled coordinate x/x_s) for smaller ϵ since x_s get larger. For consistency, we will represent in Figs. 8(d) and 8(e) the NG modes of the toy model cut at the same fixed position as in Figs. 8(a)–8(c), i.e., viewed through a window of fixed real size.

Figure 8(e) presents the results obtained from the model 1 with a fixed $\mu_1 = 0.033$ and different values of ϵ. As for the experimental results by Goujon-Durand *et al.*[2] [Fig. 8(a)] or for the numerical results by 2 [Fig. 8(c)], the growing part of the NG modes are superposed exactly into a single curve; but the tails do not coincide. This discrepancy in the tails between the toy model and the real experiment may be due either to the fact that the assumption of a linear variation of $\mu(x)$ with respect to x is crude, or to the fact that in reality μ_1 varies with ϵ. We emphasize that the theory has shown only a slight influence of the specific form of the control parameter profile on the overall structure of the pattern. At lowest order, the position x_s and amplitude A_s of the maximum remain unchanged by the variation of $\mu(x)$, which therefore induces distortions only in the far tail of the NG mode, with the constraint that the tail still follows adiabatically the variation of $\mu(x)$. A better comparison but somehow more artificial may be obtained for the tail by letting the inhomogeneity coefficient μ_1 vary with the Reynolds number [Fig. 8(d)]. The inhomogeneity parameter of our problem is estimated according to Fig. 3(b) of Ref. 3 which shows the amplitude of the transverse velocity component on the axis as a function of the streamwise position x/d (rescaled by the size of the bluff body), resulting from numerical integration
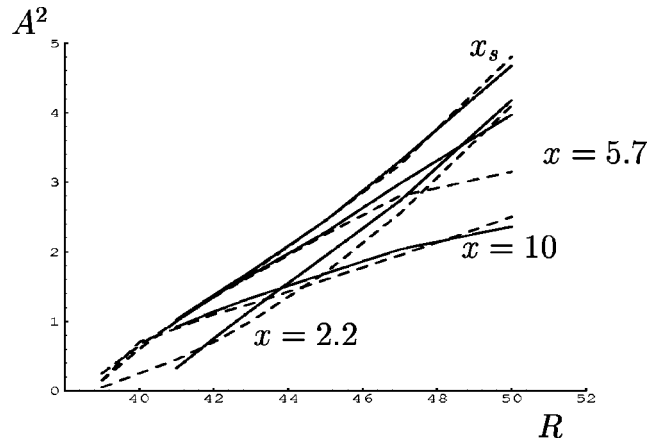

FIG. 9. A^2 at different spatial station chosen as in Ref. 3, i.e., variable $x = x_s$ and fixed $x = 2.2$, 5.7, and 10. The dotted lines represent the values reported from Fig. 5 of Ref. 3. The continuous lines represent our values computed from Eq. (12). Arbitrary units are used in the ordinate scale.

of Navier–Stokes equations for the wake configuration. For each R, a value for μ_1 is computed by assuming that downstream of x_s, the amplitude follows adiabatically the weak variation of $\sqrt{\sigma(x)}$, $\sigma(x)$ being the local linear spatial growth rate of the perturbation of the basic state. We obtain this way an estimation of the inhomogeneity parameter μ_1 which satisfies $\mu_1 \ll \epsilon^{3/2}$. The values of μ_1 vary from 0.032 for R = 41 to 0.065 for R = 50, which is coherent with the estimate previously derived from Ref. 19. In our theoretical model, we have made the hypothesis of a linear variation of $\mu(x)$ with respect to x. However, Fig. 3(b) of Ref. 3 shows that far downstream, this hypothesis certainly leads us to lose accuracy in the description of the tail of NG modes; a better quantitative agreement would have been obtained with a function $\mu(x)$ decreasing less rapidly (at a nonconstant rate). Moreover, when the Reynolds number approaches its critical value, the estimation of μ_1 becomes inaccurate as the portion of the tail computed in Ref. 3 becomes too small (for R = 39 it is even impossible to estimate the inhomogeneity of the wake as the saturation is nearly reached within the observation domain). Therefore we have used Reynolds values 41, 42, 43, 45, 47, and 50, (relative criticities from 7% to 30%) and let μ_1 vary with ϵ and plotted in Fig. 8(d) the rescaled NG modes.

The quantitative agreement is good since from the origin to twice the position of the maximum x_s, we see only slight differences between the toy model and reality.

Early exploration of the global dynamics[5] have reported Landau-like dynamics when the amplitude of the wake is measured at a fixed location. Zielinska and Wesfreid[3] have undertaken such measurements that we have reported as dashed lines in Fig. 9; we have tested such measurements using the toy model (1) with the inhomogeneity parameter varying with ϵ as in Fig. 8(d). Of course, as remarked in Ref. 3, since the global scaling (25) and (26) are not compatible with a local scaling of the amplitude in $A(x_{\text{fixed}}) \sim \sqrt{R - R_c}$, we should not observe this scaling but we want to quantify for varying μ_1 the departure of numerical results on model (1) from the classical Landau theory.

In Fig. 9, we have measured the amplitude at three different fixed distances from results of Fig. 8(e) and reported similar measurements by Zielinska and Wesfreid (Fig. 5(c) of Ref. 3). At a fixed location close to the body ($x/d = 2.2$), the amplitude varies approximately linearly with x, the slope being proportional to $f(\epsilon)$ given by Eq. (19), and therefore $A^2(x=2.2)$ possesses a parabolic shape in Fig. 9. In contrast, far enough from the origin, i.e., downstream of x_s for the ϵ reported in Fig. 9, A^2 is approximately linear with respect to R (Fig. 9 for $x=5.7$ and $x=10$) as for all the ϵ reported. Those points belong to the tail where the amplitude is locally saturated and, therefore, they follow $A^2(x_{fixed}) = \sigma_{fixed} = \mu_{fixed} = \mu_A + \epsilon - \mu_1 x_{fixed}$. Thus, if A^2 scales linearly with ϵ, the threshold value it points at is the local and not the global one: $\epsilon = \mu_1 x - \mu_A$. This analysis breaks down if the fixed position of the probe is too far in the tail. Again the quantitative agreement is fairly good, even for the highest Reynolds number (R=50). For $x = x_s(R)$, A_s^2 is linear with respect to R in agreement with Zielinska and Wesfreid results and with our extrapolation. Similar measurements using a fixed value of μ_1 would have led to similar results while the probe is between the origin and the maximum; as in Fig. 8(e) the difference from Fig. 8(d) is to be seen in the tails.

VII. CONCLUSION

In this paper we have shown that the spatial structure of nonlinear global modes in weakly inhomogeneous (nonparallel) semi-infinite systems may be described by perturbing the global mode solution we have derived for an homogeneous (parallel) semi-infinite domain and which predicts exactly with no free parameter the behavior of Rayleigh–Bénard convection[8,9] and Taylor–Couette rolls[10] with throughflow. The present model takes into account only two small parameters: the criticity ϵ of the flow and the inhomogeneity parameter μ_1. The nonlinear global modes are derived in the uniform limit where ϵ and μ_1 are brought to zero. The Landau theory based on a WKBJ approximation has been shown to be valid in an exponentially small domain of the plane (μ_1, ϵ). In contrast, this fully nonlinear theory which is essentially based on results for front propagation in homogeneous systems leads to the existence of nonlinear global modes in an entire algebraic domain of the plane (μ_1, ϵ): $\mu_1 \le \epsilon^n \forall n > \frac{3}{2}$. We have shown that a necessary condition for the existence of a fully nonlinear solution is that the saturation occurs within the locally absolutely unstable domain. In this strongly nonlinear régime, NG modes are described as fronts perturbed by the inhomogeneity only at first order in their tail, and the inner resonant layer close to the origin plays the master role of the resonator. Our main result is the existence of critical exponents for the scaling law of the maximum amplitude position, which depend on the relative magnitude of the departure from global instability threshold ϵ and of the inhomogeneity length scale. When $\mu_1 \ll \epsilon^{3/2}$, the NG mode is described at leading order as a perturbed Kolmogorov front, the scaling law for maximum amplitude location is in $1/\sqrt{\epsilon}$ and is in agreement with experimental and numerical results in wakes. In light of this result we are able to interpret the fit used for the maximum

amplitude in Refs. 2–4. In contrast, when $\epsilon^{3/2} \sim \mu_1 \ll \epsilon$ (in fact, when μ_1 exceeds the linear threshold μ_g^l by less than an exponentially small quantity), the inhomogeneity modifies the front solution at leading order and the critical exponent should change as two length scales appear in the scaling law for x_s: the length associated with the criticity parameter $\epsilon^{-1/2}$ and the inhomogeneity length scale μ_1^{-1}.

It is quite surprising that such a simple one-dimensional amplitude model may be found in agreement with experimental and numerical results since only the dynamics along the streamwise direction has been considered and simplified to the extrem. Another challenge is to explain why such a theory based on the hypothesis of a weak inhomogeneity of the medium (WKBJ type of assumption), which might appear unreasonable in the strongly nonparallel case of the wake, describes successfully, however, the spatial structure of the wake reported in the literature. Many reasons, all reflecting the crudeness of the model, may be pointed out to indicate that the model should not describe accurately the real experimental or numerical results. First, the spatial structure in the crosswise direction and the propagation of the perturbation in this crosswise direction have been neglected in the mechanism of global instability. This crosswise direction is considered to be slave to the dynamics in the streamwise direction. Second, our model is minimal in the sense that it takes into account only the leading order terms in x, k, and R necessary to produce a nonlinear global instability. The linear part of the model represents the simplest dispersion relation with one temporal branch and two spatial branches leading to a change of nature of the instability (transition from convective to absolute instability). The cubic nonlinearity is the leading order nonlinear term compatible with translational invariance in time. The reason for the ability of the present theoretical approach to describe real experiments, even if the parameters are driven far beyond the validity domain of the theory, is perhaps due to these essential ingredients which capture the main features of conserved symmetries or broken symmetries of the real flow.

In Ref. 2, it is suggested that the experimentally observed scaling laws could be explained by a model of Ginzburg–Landau equation with complex coefficients. We have studied in Ref. 29 the structure of homogeneous NG modes of the complex Ginzburg–Landau equation with cubic nonlinearities and we have shown that although the model is no longer potential, the homogeneous NG modes have the structure of a front selected by the linear marginal stability criteria, and exhibit a growth length which scales like $\epsilon^{-1/2}$, as for the real Ginzburg–Landau model. As scaling laws for all the length scales introduced in Sec. II keep being identical when the complete Ginzburg–Landau equation is considered instead of the real one, the structure of the NG mode would be similar in both cases. The only novel results would be the frequency selection, which should be similar at leading order to the homogeneous case described in Ref. 29. For the maximum amplitude value and location, the scaling laws should only differ by numerical factors depending upon the imaginary parts of the Ginzburg–Landau coefficients. Associated with the derivation of those coefficients for the experimental setup used in Ref. 2, this study

Phys. Fluids, Vol. 11, No. 12, December 1999

Fully nonlinear global modes in slowing varying flows   3701

should lead to a systematic quantitative comparison between our theory and the experiment. However, if the imaginary parts of the Ginzburg–Landau coefficients are small (as for the Rayleigh–Bénard or the Taylor–Couette experiment), the real model should give very good quantitative agreement between theory and experiment (as it is already the case when the flow is parallel, as we have demonstrated in Ref. 29).

Similar ideas have been recently developed to explain the occurence of self-sustained resonances in galactic disks and stellar shells. See the review article by Soward[47] for extensive references, and in particular Refs. 48–51. In this case, two coupled equations describe the dynamics of the magnetic field; self-sustained resonances occur when the propagative waves become absolutely unstable; the spatial structure consists of a front stabilized at the location of the convective/absolute transition.

APPENDIX A: DETAILED SPATIAL STRUCTURE OF NG MODES

1. Outer layer CNL

In this subdomain, the NG mode has saturated and its saturation amplitude follows the weak variation of the control parameter with respect to x. On using the change of variable

$$Z = \mu_1 x - \mu_0, \tag{A1}$$

where $\mu_0 = \mu_A + \epsilon$ and $\mu_1 = \epsilon^n$, we can rewrite Eq. (12) up to the second order in the form

$$ZA(Z) + A^3(Z) + \epsilon^n U_0 A'(Z) = 0, \tag{A2}$$

where a prime denotes differentiation with respect to the argument. The solution of Eq. (A2) reads

$$A(Z) = \sqrt{-Z} + \epsilon^n \frac{U_0}{4(-Z)^{3/2}} \tag{A3}$$

and represents the saturation amplitude which follows the weak variation of $\mu(x)$ with respect to x. By making use of (A1), we obtain $Z = -\mu_A - \epsilon + \epsilon^n x$, and expansion of (A3) in powers of ϵ yields

$$A \simeq \sqrt{\mu_A} - \epsilon^n \frac{1}{2\sqrt{\mu_A}} x + \epsilon \frac{1}{2\sqrt{\mu_A}} + \epsilon^n \frac{U_0}{4\mu_A^{3/2}}. \tag{A4}$$

2. Transition layer TL^s

Around the saturation amplitude, $A = A_2(\mu_A) - \epsilon^p \phi(x)$, where $\phi(x)$ satisfies the equation obtained by linearizing (12) around $A_2 \equiv A_2(\mu_A)$:

$$\frac{d^2\phi}{dx^2} - U_0 \frac{d\phi}{dx} + \mu_2 \phi = (\epsilon^{1-p} - \epsilon^{n-p} x) A_2, \tag{A5}$$

where $\mu_2 = \mu_A - 3A_2^2 = -2\mu_A$. [For clarity, we no longer explicitly mention the (μ_A) dependence of $A_2 \equiv A_2(\mu_A) = \sqrt{\mu_A}$.] Using the notations

$$k_- = \frac{U_0(1-\sqrt{3})}{2}, \quad k_+ = \frac{U_0(1+\sqrt{3})}{2}, \tag{A6}$$

the general solution of Eq. (A5) then reads

$$\phi(x) = c_1 e^{k_+(x-x_s)} + c_2 e^{k_-(x-x_s)}$$
$$+ \epsilon^{1-p} \frac{A_2}{\mu_2} - \epsilon^{n-p} \frac{A_2}{\mu_2}\left(x + \frac{U_0}{\mu_2}\right), \tag{A7}$$

where the last non-exponential term represents a particular solution of (A5) and c_1, c_2 are integration constants. A boundary condition will be imposed by the matching when $x - x_s \to +\infty$. The outer solution (A4) in CNL is linear with respect to x; then $\epsilon^p \phi(x)$ must be also linear when $x - x_s \to +\infty$. This matching condition implies $c_1 = 0$. As $x - x_s \to +\infty$, the inner solution (A7) admits the expansion

$$\epsilon^p \phi(x) \simeq \frac{A_2}{\mu_2}\left(-\epsilon^n x + \epsilon - \epsilon^n \frac{U_0}{\mu_2}\right) \tag{A8}$$

Since $A_2 = \sqrt{\mu_A}$ and $\mu_2 = -2\mu_A$, expansion (A8) represents exactly orders ϵ and ϵ^n of (A4). Matching between CNL and TL^s is done.

The position of the maximum x_s must satisfy the condition $d\phi/dx(x_s) = 0$, which determines the constant $c_2 = \epsilon^{n-p} A_2 / \mu_2 k_-$. The complete solution (A7) then reads

$$\phi(x) = \epsilon^{-p} \frac{A_2}{\mu_2}\left(\frac{\epsilon^n}{k_-} e^{k_-(x-x_s)} + \epsilon - \epsilon^n\left(x + \frac{U_0}{\mu_2}\right)\right). \tag{A9}$$

When $x - x_s \to -\infty$, the asymptotic behavior of $\phi(x)$ is determined by the exponential term. On differentiating Eq. (A9) and using again (A9) in order to eliminate $e^{k_-(x-x_s)}$, it follows that

$$\epsilon^p \frac{d\phi}{dx} = k_- \epsilon^p \phi + \frac{k_- A_2}{\mu_2}\left(\epsilon^n x_s - \epsilon + \epsilon^n\left(\frac{U_0}{\mu_2} - \frac{1}{k_-}\right)\right). \tag{A10}$$

This exact relation will, however, be used as the asymptotic behavior of the solution (A9) in the phase space as $x - x_s \to -\infty$. Moreover, the maximum amplitude verifies $A(x_s) = A_2 - \epsilon^p \phi(x_s)$ with

$$\epsilon^p \phi(x_s) = -\epsilon^n \frac{A_2}{\mu_2} x_s + \epsilon \frac{A_2}{\mu_2} + \epsilon^n \frac{A_2}{\mu_2}\left(\frac{1}{k_-} - \frac{U_0}{\mu_2}\right). \tag{A11}$$

3. Layer KF

The solution is sought directly in the phase space in the form of a series representing $u(A) \equiv dA/dx$ and expanded into

$$u(A) = \frac{dA}{dx} = u_0(A) + \epsilon u_1(A) + \mu_1 u_2(x, A). \tag{A12}$$

At the lowest order in ϵ, let us briefly recall how to compute $u_0(A)$, which is the same solution as the one obtained for

saturated global modes,[28] i.e., linking the origin of phase space $(A=0, dA/dx=0)$ to the point $(A=A_2(\mu_A), dA/dx=0)$ and satisfying

$$u_0 u_0' - U_0 u_0 + \mu_A A - A^3 = 0, \tag{A13}$$

where a prime denotes differentiation with respect to A. This solution reads

$$u_0(A) = -\sum_{j=1}^{+\infty} \nu_j (A_2 - A)^j. \tag{A14}$$

Introduction of (A14) in (A13) and identification of the powers of $(A_2 - A)$ yield equations for the recursive coefficients ν_j which may be numerically computed. [The first one at lowest order in $(A_2 - A)$ must be negative since (A14) represents the stable manifold of A_2 and satisfies $\nu_1^2 - U_0 \nu_1 + \mu_2 = 0$. Thus $\nu_1 = U_0(1 - \sqrt{3})/2 \equiv k_-$.]

Here $u_1(A)$ and $u_2(x, A)$ satisfy

$$u_0 \partial_A u_1 + (\partial_A u_0 - U_0) u_1 = -A, \tag{A15}$$

$$u_0 \partial_A u_2 + \partial_x u_2 + (\partial_A u_0 - U_0) u_2 = xA, \tag{A16}$$

and are also sought in the form of series expansions

$$u_1(A) = -\sum_{j=0}^{+\infty} \lambda_j (A_2 - A)^j, \tag{A17}$$

$$u_2(x, A) = \sum_{j=0}^{+\infty} (\zeta_j + \eta_j x)(A_2 - A)^j. \tag{A18}$$

The recurrent coefficients λ_j, ζ_j, and η_j are numerically computed. [The first equations allowing to initiate the computation read

$$(U_0 - \nu_1)\lambda_0 = A_2, \quad \text{or} \quad \lambda_0 = (1 + \sqrt{3})^{-1},$$

$$(U_0 - \nu_1)\eta_0 = -A_2, \quad \text{or} \quad \eta_0 = -(1 + \sqrt{3})^{-1},$$

$$(U_0 - \nu_1)\zeta_0 = \eta_0, \quad \text{or} \quad \zeta_0 = -U_0^{-1}(2 + \sqrt{3})^{-1}.]$$

The asymptotic behavior of the solution (A12) as $A \to A_2$ in the phase space reads

$$\frac{dA}{dx} \simeq -\nu_1(A_2 - A) + \mu_1 x \eta_0 + \epsilon \lambda_0 + \mu_1 \zeta_0. \tag{A19}$$

Since we have verified that

$$k^- = \nu_1, \quad \frac{k_- A_2}{\mu_2} = -\eta_0 = \lambda_0, \quad \zeta_0 = \left(1 - \frac{U_0 k_-}{\mu_2}\right)\frac{A_2}{\mu_2},$$

expansions (A19) and (A10) are identical whatever p and solutions in TL^s and KF are now matched. In other words, the matching succeeds whatever the size of the transition layer TL^s.

When $A \to 0$, the asymptotic behavior of the solution reads

$$u_0(A) + \epsilon u_1(A) + \mu_1 u_2(x, A)$$

$$\simeq -\sum_{j=1}^{+\infty} \nu_j A_2^j + \sum_{j=1}^{+\infty} j \nu_j A_2^{j-1} A + \mu_1 x \sum_{j=0}^{+\infty} \eta_j A_2^j$$

$$- \epsilon \sum_{j=0}^{+\infty} \lambda_j A_2^j + \mu_1 \sum_{j=0}^{+\infty} \zeta_j A_2^j. \tag{A20}$$

4. Transition layer TL⁰ and outer layer OL

In the outer layer OL^+, $A(x)$ is small since it must vanish at infinity. Therefore, $A(x)$ is the solution of the linear equation (13) and reads

$$A(x) = g(\mu_1)\exp\left(\frac{U_0}{2}x\right)\text{Ai}((x - x_A)\mu_1^{1/3}) \tag{A21}$$

where $g(\mu_1)$ is an integration constant (the coefficient of Bi must be zero in order to cancel the growing part of the general solution).

In the central nonlinear layer CNL, when $Z \to 0$, a singularity appears in the solution (A3). The transition layer TL^0 has therefore been introduced to match solutions (A3) and (A21) when $Z \to 0$. In this layer, on using the change of variable $\tilde{Z} = Z/\mu_1^{1/2}$ and $A(Z) = \mu_1^{1/4}\tilde{A}(\tilde{Z})$ in order to collect the nonlinear term, the advection term, and the inhomogeneous term at the same order, $\tilde{A}(\tilde{Z})$ satisfies

$$U_0 \tilde{A}' = -\tilde{Z}\tilde{A} - \tilde{A}^3. \tag{A22}$$

The solution of Eq. (A22) reads

$$\tilde{A} = \tilde{A}_0\left(1 + \frac{2\tilde{A}_0^2}{U_0}\int_0^{\tilde{Z}} e^{-u^2/U_0}\,du\right)^{-1/2} e^{-\tilde{Z}^2/2U_0}, \tag{A23}$$

where the integration constant $\tilde{A}_0$ is given by the matching with the CNL solution. Indeed, as $\tilde{Z} \to -\infty$, we obtain

$$\tilde{A} \simeq \sqrt{-\tilde{Z}}\left(1 + \frac{U_0}{4\tilde{Z}^2}\right) \tag{A24}$$

if the choice $\tilde{A}_0 = (U_0/\pi)^{1/4}$ is done and solution (A24) matches with (A3).

When $\tilde{Z} \to +\infty$, the solution (A23) admits the asymptotic expansion

$$\tilde{A} \simeq \frac{\tilde{A}_0}{\sqrt{2}} = \left(\frac{U_0}{4\pi}\right)^{1/4}\exp\left(-\frac{\tilde{Z}^2}{2U_0}\right) \tag{A25}$$

and matches with the OL solution (A21) once the following value of $g(\mu_1)$ is chosen:

$$g(\mu_1) = \pi^{1/4}U_0^{3/4}\exp\left(-\frac{U_0^3}{24\mu_1}\right). \tag{A26}$$

[1] P. Huerre and P. A. Monkewitz, ''Local and global instabilities in spatially developing flows,'' Annu. Rev. Fluid Mech. **22**, 473 (1990).

[2] S. Goujon-Durand, P. Jenffer, and J. E. Wesfreid, ''Downstream evolution of the Bénard-von Kármán instability,'' Phys. Rev. E **50**, 308 (1994).

[3] B. J. A. Zielinska and J. E. Wesfreid, ''On the spatial structure of global modes in wake flow,'' Phys. Fluids **7**, 1418 (1995).

[4] J. E. Wesfreid, S. Goujon-Durand, and B. J. A. Zielinska, ''Global mode

behavior of the streamwise velocity in wakes,'' J. Phys. II France **6**, 1343 (1996).

[5] C. Mathis, M. Provansal, and L. Boyer, ''The Bénard von Kármán instability: an experimental study near the threshold,'' J. Phys. Lett. (Paris) **45**, 483 (1984).

[6] K. R. Sreenivasan, S. Raghu, and D. Kyle, ''Absolute instability in variable density round jets,'' Exp. Fluids **7**, 309 (1989).

[7] P. J. Strykowski and D. L. Niccum, ''The influence of velocity and density ratio on the dynamics of spatially developing mixing layers,'' Phys. Fluids A **4**, 770 (1992).

[8] H. W. Müller, M. Lücke, and M. Kamps, ''Convective patterns in horizontal flow,'' Europhys. Lett. **10**, 451 (1989).

[9] H. W. Müller, M. Lücke, and M. Kamps, ''Transversal convection patterns in horizontal shear flow,'' Phys. Rev. A **45**, 3714 (1992).

[10] P. Büchel, M. Lücke, D. Roth, and R. Schmitz, ''Pattern selection in the absolutely unstable regime as a nonlinear eigenvalue problem: Taylor vortices in axial flow,'' Phys. Rev. E **53**, 4764 (1996).

[11] D. Rockwell and E. Naudascher, ''Self sustained oscillations of impinging free shear layers,'' Annu. Rev. Fluid Mech. **11**, 67 (1979).

[12] E. Villermaux, ''Auto-oscillation et mélange dans les écoulements reciculants,'' Thèse de doctorat, Université de Paris VI, 1993.

[13] W. Koch, ''Local instability characteristics and frequency determination of self excited wake flows,'' J. Sound Vib. **99**, 53 (1985).

[14] R. J. Briggs, *Electron-Stream Interaction with Plasmas* (MIT, Cambridge, MA, 1964).

[15] A. Bers, ''Observation on vorticity creation boundary condition,'' in *Physique des Plasmas*, edited by C. De Witt and J. Peyraud (Gordon and Breach, New York, 1975), pp. 117–215.

[16] E. M. Lifshitz and L. P. Pitaevskii, *Physical kinetics* (Pergamon, London, 1981).

[17] P. A. Monkewitz, P. Huerre, and J.-M. Chomaz, ''Global linear stability analysis of weakly non parallel shear flows,'' J. Fluid Mech. **251**, 1 (1993).

[18] J.-M. Chomaz, P. Huerre, and L. G. Redekopp, ''Bifurcations to local and global modes in spatially developing flows,'' Phys. Rev. Lett. **60**, 25 (1988).

[19] D. A. Hammond and L. G. Redekopp, ''Global dynamics of symmetric and asymmetric wakes,'' J. Fluid Mech. **338**, 231 (1997).

[20] If more than two spatial branches are present as in the case of a water jet with surface tension, feedback mechanism which involves more than one branch may also lead to a self-sustained resonance as demonstrated by Yakubenko (Ref. 46).

[21] J.-M. Chomaz, P. Huerre, and L. G. Redekopp, ''A frequency selection criterion in spatially developing flows,'' Stud. Appl. Math. **84**, 119 (1991).

[22] The name ''WKBJ'' follows the names of authors (Wentzel, Kramers, Brillouin, and Jeffrey) who have developed this approximation method. See Ref. 42 for details.

[23] J.-M. Chomaz, P. Huerre, and L. G. Redekopp, ''The effect of nonlinearity and forcing on global modes,'' in *New Trends in Nonlinear Dynamics and Pattern-forming Phenomena*, edited by P. Coullet and P. Huerre (Plenum, New York, 1990).

[24] S. Le Dizès, P. Huerre, J.-M. Chomaz, and P. A. Monkewitz, ''Nonlinear stability analysis of slowly-diverging flows: Limitations of the weakly nonlinear approach,'' in *Proceedings of the IUTAM Symposium on Bluff-body Wakes, Dynamics and Instabilities*, edited by H. Eckelmann, J. M. R. Graham, P. Huerre, and P. A. Monkewitz (Springer Verlag, New York, 1993).

[25] Y. Pomeau, S. Zaleski, and P. Manneville, ''Axisymmetric cellular structures revisited,'' Z. Angew. Math. Phys. **36**, 367 (1985).

[26] J.-M. Chomaz, ''Absolute and convective instabilities in nonlinear systems,'' Phys. Rev. Lett. **69**, 1931 (1992).

[27] A. Couairon and J.-M. Chomaz, ''Global instability in nonlinear systems,'' Phys. Rev. Lett. **77**, 4015 (1996).

[28] A. Couairon and J.-M. Chomaz, ''Absolute and convective instabilities, front velocities and global modes in nonlinear systems,'' Physica D **108**, 236 (1997).

[29] A. Couairon and J.-M. Chomaz, ''Pattern selection in the presence of a cross flow,'' Phys. Rev. Lett. **79**, 2666 (1997).

[30] A. Couairon and J.-M. Chomaz, ''Primary and secondary nonlinear global instability,'' Physica D **132**, 428 (1999).

[31] J.-M. Chomaz and A. Couairon, ''Against the wind,'' Phys. Fluids **11**, 2977 (1999).

[32] A. Kolmogorov, I. Petrovsky, and N. Piskunov, ''Investigation of a diffusion equation connected to the growth of materials, and application to a problem in biology,'' Bull. Univ. Moscow, Ser. Int. Sec. A **1**, 1 (1937).

[33] G. Dee, ''Dynamical properties of propagating front solutions of the amplitude equations,'' Physica D **15**, 295 (1985).

[34] G. Dee, ''Propagation into an unstable state,'' J. Stat. Phys. **39**, 705 (1985).

[35] W. van Saarloos, ''Front propagation into unstable states: marginal stability as a dynamical mechanism for velocity selection,'' Phys. Rev. A **37**, 211 (1988).

[36] H. Chaté and P. Manneville, ''Phase diagram of the two-dimensional complex Ginzburg–Landau equation,'' Physica A **224**, 348 (1996).

[37] C. M. Ho and P. Huerre, ''Perturbed shear layers,'' Annu. Rev. Fluid Mech. **16**, 365 (1984).

[38] R. E. Hunt, ''Spatially varying flows with localized forcing,'' Ph.D. thesis, Trinity College, Cambridge, 1995.

[39] R. E. Hunt and D. G. Crighton, ''Instability of flows in spatially developing media,'' Proc. R. Soc. London, Ser. A **435**, 109 (1991).

[40] D. A. Hammond and L. G. Redekopp, ''Global dynamics and flow vectoring in asymmetric wakes,'' AIAA Paper No. 94-2219, 1994.

[41] J.-M. Chomaz, P. Huerre, and L. G. Redekopp, ''Models of hydrodynamic resonances in separated shear flows,'' in *Proceedings of the Sixth Symposium on Turbulent Shear Flows*, Toulouse, France, 1987, pp. 321–326.

[42] C. M. Bender and S. A. Orszag, ''Advanced Mathematical Methods for Scientists and Engineers'' (McGraw Hill, New York, 1978).

[43] B. Pier and P. Huerre, ''Fully nonlinear global modes in spatially developing media,'' Physica D **97**, 206 (1996); B. Pier, P. Huerre, J.-M. Chomaz, and A. Couairon, ''Steep nonlinear global modes in spatially developing media,'' Phys. Fluids **10**, 2433 (1998).

[44] M. Abramowitz and I. A. Stegun, *Handbook of Mathematical Functions* (Dover, New York, 1972).

[45] P. Albarède and P. A. Monkewitz, ''A model for the formation of oblique shedding and ''chevron'' patterns in cylinder wakes,'' Phys. Fluids A **4**, 744 (1992).

[46] P. A. Yakubenko, ''Global capillary instability of an inclined jet,'' J. Fluid Mech. **346**, 181 (1997).

[47] A. M. Soward, ''Thin aspect ratio $\alpha\Omega$-dynamos in galactic disks and stellar shells,'' to appear in *Advances in Nonlinear Dynamos,* edited by M. Nunez and A. Fertiz Mas. Book series: *The Fluid Mechanics of Astrophysics and Geophysics.*

[48] A. P. Bassom, K. M. Kuzanyan, and A. Soward, ''A nonlinear dynamo wave riding on a spatially varying background,'' Proc. R. Soc. London, Ser. A **A455**, 1443 (1999).

[49] N. Meunier, M. R. E. Proctor, D. Sokoloff, A. M. Soward, and S. M. Tobias, ''Asymptotic properties of a nonlinear $\alpha\omega$-dynamo wave: Period, amplitude, and latitude dependence,'' Geophys. Astrophys. Fluid Dyn. **86**, 249 (1997).

[50] S. M. Tobias, M. R. E. Proctor, and E. Knobloch, ''The role of absolute instability in the solar dynamo,'' Astron. Astrophys. **318**, L55 (1997).

[51] S. M. Tobias, M. R. E. Proctor, and E. Knobloch, ''Convective and absolute instabilities of fluid flows in finite geometry,'' Physica D **113**, 43 (1998).